

Investigating the Potential of LS 5039 as a Triple System Using Fermi-LAT Data

LUJUN ZENG,¹ MENGQING ZHANG,¹ CHONGYANG REN,^{2,3} PENGFEI ZHANG,¹ AND JINGZHI YAN^{2,3}

¹*Department of Astronomy, School of Physics and Astronomy, Key Laboratory of Astroparticle Physics of Yunnan Province, Yunnan University, Kunming 650091, People's Republic of China; zhangpengfei@ynu.edu.cn*

²*Key Laboratory of Dark Matter and Space Astronomy, Purple Mountain Observatory, Chinese Academy of Sciences, Nanjing 210034, People's Republic of China; jzyan@pmo.ac.cn*

³*School of Astronomy and Space Science, University of Science and Technology of China, Hefei, Anhui 230026, People's Republic of China*

ABSTRACT

LS 5039 is one of a handful of γ -ray binary systems in the Milky Way, comprising a pulsar and a massive O-type companion star with an orbital period of 3.9 day. Recently, we conducted a data analysis using approximately 16 year of Fermi-LAT observations, spanning from 2008 August 4 to 2024 July 8. In our timing analysis, we discovered two new periodic signals with frequencies higher and lower than the known orbital period. The higher-frequency signal has a period of 3.63819 day with a 7.1σ confidence level, while the lower-frequency signal has a period of 4.21654 day with a 6.3σ confidence level. Additionally, in data from the High Energy Stereoscopic System of Cherenkov Telescopes, two potential signals with periods similar to the two newly discovered ones. Considering that these two signals fall within the same frequency interval as the orbital period, we suggest the possibility of a third body orbiting the barycenter of the LS 5039 binary system, with the new periodic signals arising from specific frequency combinations of the two orbital periods.

Keywords: Gamma-rays(637); Gamma-ray sources(633); Periodic variable stars(1213)

1. INTRODUCTION

To date, only a few γ -ray binary systems have been identified in our Galaxy (Aharonian et al. 2006; Albert et al. 2006; Hinton et al. 2009; Fermi LAT Collaboration et al. 2012a; Li et al. 2017; Corbet et al. 2019), with LS 5039 being one of them. LS 5039 is a well-studied high-mass X-ray binary, consisting of a rapidly rotating neutron star with a spin period of 9 s (Yoneda et al. 2020) and a massive O-type companion star (Maíz Apellániz et al. 2016) with a mass of $23 M_{\odot}$ (Casares et al. 2005a). The two objects orbit each other with a period of 3.9 day in a moderately eccentric orbit with an eccentricity of 0.35 and an orbital inclination of $i = 25^{\circ}$, at a distance of 2.5 kpc from Earth within our Galaxy (Casares et al. 2005a). The orbital phase zero (i.e. ϕ_0) is defined at its periastron passage, with the reference epoch T_0 set at HJD 2451943.09 (i.e. MJD 51942.59; Casares et al. 2005a). Notably, LS 5039 is one of only three known γ -ray binary systems in which the compact object is a neutron star, the other two being LS I + $61^{\circ}303$ (Weng et al. 2022) and PSR B1259–63/SS 2883 (Johnston et al. 1992).

LS 5039's electromagnetic emissions span a broad spectrum, ranging from radio frequencies to TeV γ -ray energies (Moldón et al. 2012; Casares et al. 2005a; Takahashi et al. 2009; Abdo et al. 2009; Aharonian et al. 2006) and potentially reaching PeV (Cao et al. 2021; Bykov et al. 2024). Its spectral energy distribution, which is dominated by MeV-GeV γ -rays, characterizes LS 5039 as a γ -ray binary. The 3.9 day orbital modulation of LS 5039 has been identified by multi-wavelength observations and is well-supported by extensive literature. Notably, at energies above 0.1 TeV, Aharonian et al. (2006) presented its orbital modulation with a period of 3.9078 ± 0.0015 day based on the dataset from the High Energy Stereoscopic System (HESS) of Cherenkov Telescopes. In GeV, LS 5039 was detected by Abdo et al. (2009) using the 11 month *Fermi*-LAT observations, who also reported that its γ -ray emissions are modulated by a 3.903 ± 0.005 day orbital period. Recently, Zhang (2024) discovered a new periodic signal with a period of 26.3 day in the γ -ray binary LS I + $61^{\circ}303$ using *Fermi*-LAT observations. Motivated by these findings, we conducted a new timing analysis of LS 5039, hoping

Table 1. Results of likelihood

Models	Parameter values				
LP	α	β	E_b	TS	F_{ph}
	2.758	0.102	2.0		
	2.701(3)	0.036(1)	2.0	29003.2	7.46(9)
PLEC	Γ	b	E_c	TS	F_{ph}
	2.511(16)	2/3	13.9(31)	28912.7	7.46(17)

Notes. Best-fit parameters of the likelihood, F_{ph} in unit of $\times 10^{-7}$ photons $\text{cm}^{-2} \text{s}^{-1}$, E_b and E_c in unit of GeV.

to uncover phenomena beyond its known orbital period in GeV gamma-rays.

In the fourth catalog Data Release 4 (4FGL-DR4; Ballet et al. 2023), LS 5039 is associated with the γ -ray counterpart 4FGL J1826.2–1450, which has been monitored by Fermi-LAT for approximately 16 year. In our timing analysis, in addition to the detection of the orbital period of 3.90609 day, we identified two new periodic signals with frequencies higher and lower than the orbital period. These signals have periods of 3.63819 day and 4.21654 day, with confidence levels of 7.1σ and 6.3σ , respectively. Moreover, two similar periodic signals were observed in data from the HESS of Cherenkov Telescopes (Aharonian et al. 2006). The details of our data analysis and findings are presented below. In them, the numbers in parentheses indicate the uncertainties associated with the values.

2. DATA ANALYSIS AND RESULTS

2.1. Data Reduction

For our data analysis, we utilized the Pass 8 *Front+Back* events (evclass = 128 and evtype = 3), focusing on the energy range of 0.1–500.0 GeV within a $20^\circ \times 20^\circ$ region of interest centered on 4FGL J1826.2–1450 (R.A. = 276.5637, Decl. = -14.8496), covering the period from MJD 54682.687 to 60499.299. Events with zenith angles $< 90^\circ$ were selected, and only high-quality events from good time intervals were retained using the expression “DATA_QUAL>0 && LAT_CONFIG==1”. The Galactic and isotropic diffuse emissions were modeled using the templates of gll_iem_v07.fits and iso_P8R3_SOURCE_V2_v1.txt, respectively. The data was reduced and analyzed using the FermiTools version 2.2.0.

A model file was created based on 4FGL-DR4, and a binned maximum likelihood analysis was performed to update the model parameters. For 4FGL J1826.2–1450, the 4FGL-DR4 provides a log-parabola (LP) spec-

tral shape, $dN/dE = N_0(E/E_b)^{-[\alpha+\beta \log(E/E_b)]}$. Additionally, we also employed a power-law with an exponential cutoff (PLEC) model, $dN/dE = N_0(E/E_0)^{-\Gamma} \exp[-(E/E_c)^b]$, to fit the events around 4FGL J1826.2–1450. All parameters for these two models are summarized in Table 1. As shown in it, we conclude that the LP model, which yields a higher TS value of 29,003.2, provides a better representation of the γ -ray emissions from LS 5039 compared to the PLEC model, which has a TS value of 28,912.7. The LP model results were then saved as the best-fit model. Based on it, we generated a TS map for 4FGL J1826.2–1450’s γ -ray emissions (see left panel of Figure 1) and a residual TS map excluding γ -rays from all sources listed in the 4FGL-DR4 (right panel of Figure 1). These maps indicate that the γ -ray emissions from 4FGL J1826.2–1450 is well-described by the LP model.

2.2. Light Curve Construction and Timing Analysis

A modified version of the aperture photometry (AP) method was employed to construct the light curve for 4FGL J1826.2–1450 in the 0.1–500.0 GeV. To optimize the signal-to-noise ratio, an aperture radius of $3^\circ.16$ was selected, taking into account the performance characteristics of the LAT instrument, with a criterion of $\theta < \max(6.68 - 1.76 \log_{10}(E_{\text{MeV}}), 1.3)^\circ$, 1.3), following that performed in Abdo et al. (2010). The light curve was binned at 500 s intervals for each time bin. To mitigate contamination from γ -rays originating from the Sun and Moon, we excluded events occurring when the target was within 5° of either the Sun or the Moon, using *gtmktime*. To address significant exposure time variations across different time bins, the exposure time for each bin was calculated using *gtexposure*. Using the best-fit model, event probabilities for 4FGL J1826.2–1450 were determined by employed *gtsrcreprob* and used as weights for constructing the AP light curve, rather than simply counting photon numbers (Kerr 2011; Fermi LAT Collaboration et al. 2012b; Corbet et al. 2019). Additionally, the times in the light curve were corrected to the barycenter using *gtbary*.

In our timing analysis, a method of the generalised Lomb–Scargle periodogram (LSP; Lomb 1976; Scargle 1982; Zechmeister & Kürster 2009) was employed to derive the power spectrum for the AP light curve. Compare to other period search algorithms, the LSP offers more accurate frequency determination for unevenly spaced data, is less susceptible to aliasing, provides better frequency resolution, improves the detection of weak signals, and facilitates the assessment of the confidence level for periodic signals. This same methodology was

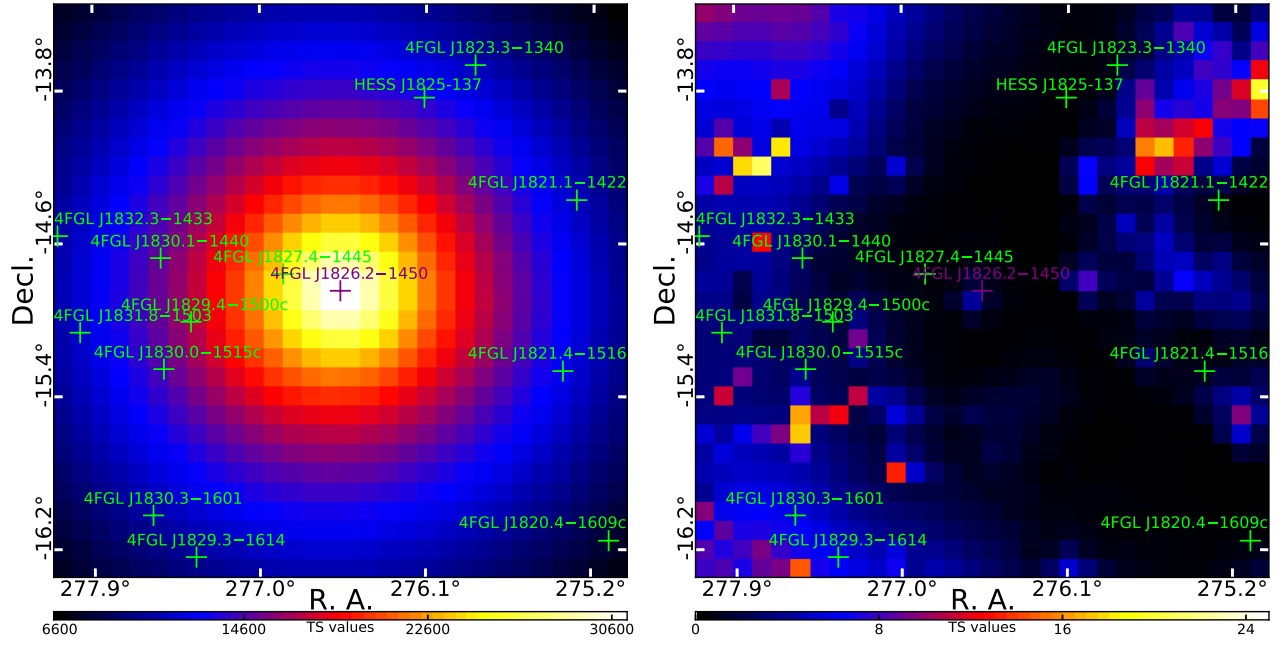


Figure 1. TS maps in the 0.1–500.0 GeV range, covering a $3^\circ \times 3^\circ$ region centered on 4FGL J1826.2–1450, with γ -ray sources from the 4FGL-DR4 marked by crosses. Left panel: TS map representing γ -ray emissions from 4FGL J1826.2–1450, generated using the best-fit model with the target excluded. Right panel: Residual TS map created using the same model, except with 4FGL J1826.2–1450 included.

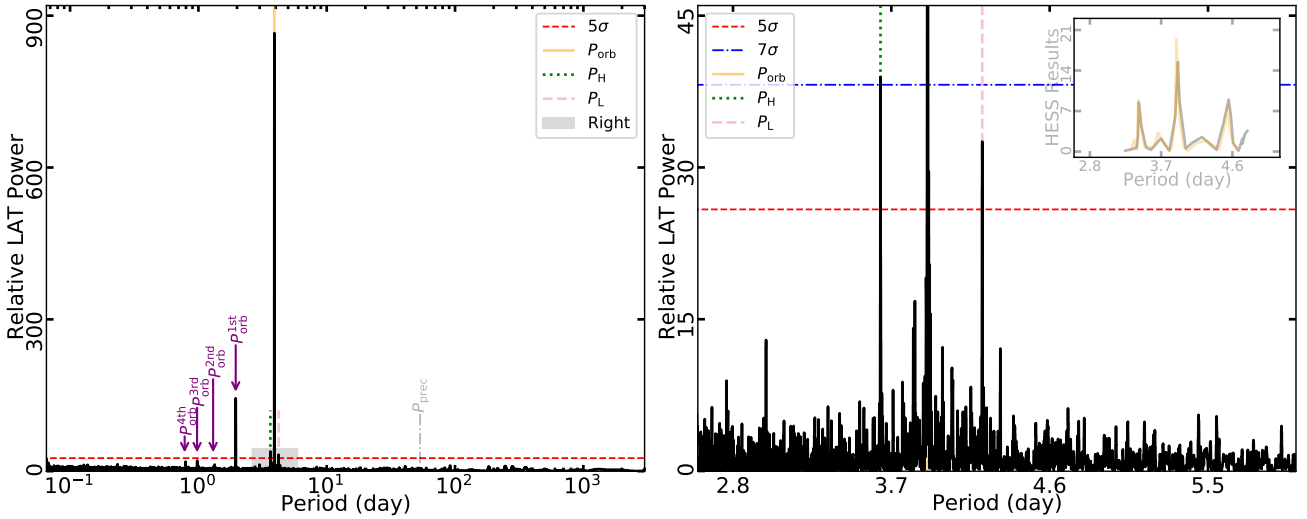


Figure 2. LSP power spectra (black histogram) derived from the 0.1–500.0 GeV AP light curve of 4FGL J1826.2–1450. Left panel: The three periodicities, P_H , P_{orb} , and P_L , are in close proximity. The gray dashed-dotted line marks the location of the 53.4 day precession period of the *Fermi*-LAT orbit. Right panel: LSP power spectrum zoomed in the left. The green dotted and pink dashed lines indicate the signals of P_H and P_L , respectively. The horizontal red dashed and blue dashed-dotted lines stand for 5σ and 7σ confidence levels. HESS results that drawn from the Figures 2 and 3 of Aharonian et al. (2006) are shown in the inset plot.

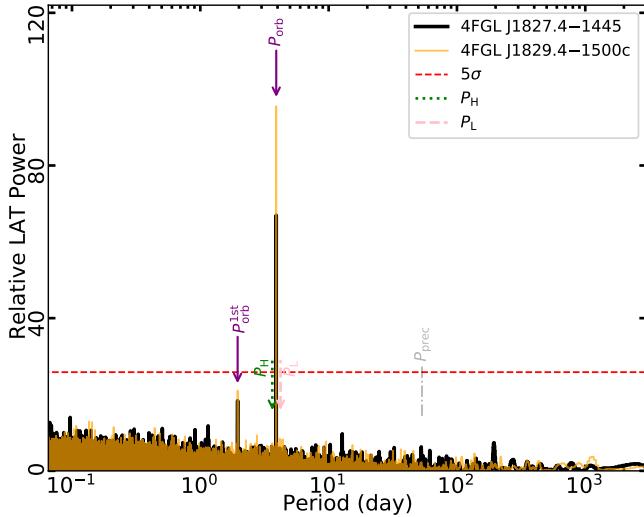


Figure 3. LSP power spectra for 4FGL J1827.4–1445 (black histogram) and 4FGL J1829.4–1500c (orange histogram). The vertical green and pink arrows show the positions of the two signals of P_H and P_L . The gray dashed-dotted line is the precession period of the *Fermi*-LAT orbit. And the red dashed line is 5σ confidence level.

also employed by Zhang (2024). The power spectrum covers a frequency range from $f_{\max} = 1/0.06 \text{ day}^{-1}$ to $f_{\min} = 1/5816.612 \text{ day}^{-1}$ (e.g., the inverse of the length of *Fermi*-LAT observations, $1/T_{\text{obs}}$). We show the power spectrum in left panel of Figure 2, in it a prominent main peak appears at 3.90609(3) day, corresponding to the orbital period (P_{orb}) of LS 5039. In addition to P_{orb} , two peaks can be observed on either side of it. One period appears at the higher frequency with period of 3.63819(14) day (P_H) and another at the lower frequency at 4.21654(20) day (P_L). For the three periods, their uncertainties were calculated by $\delta P = \frac{3}{8} \frac{P^2}{T_{\text{obs}} \sqrt{p_n}}$, where P is a period, T_{obs} is the length of *Fermi*-LAT observations, and p_n is the normalized height of the peak power, as that provided in Horne & Baliunas (1986). These periods, P_{orb} , P_H , and P_L , correspond to frequencies of $f_{\text{orb}} = 0.256010(2) \text{ day}^{-1}$, $f_H = 0.274862(10) \text{ day}^{-1}$, and $f_L = 0.237161(11) \text{ day}^{-1}$, respectively. Moreover, the frequency difference between P_H and P_{orb} ($f_H - f_{\text{orb}} = 0.018851$) is nearly equal to the difference between P_{orb} and P_L ($f_{\text{orb}} - f_L = 0.018849$). In left panel of Figure 2, we marked the P_{orb} , P_H , and P_L with orange solid, green dotted, and pink dashed lines, respectively. And the first, second, third, and fourth harmonics of P_{orb} also appear, we mark them with four purple arrows. For clarity we zoom in the power spectrum in the gray shaded region in right panel of Figure 2.

The heights of the peaks of P_{orb} , P_H and P_L are ~ 865.88 , ~ 36.38 , and ~ 33.10 , respectively, compared to the mean power level, based on the normalization

provided in Horne & Baliunas (1986). For P_H and P_L , the probabilities (p_{isp}) of a periodic signal reaching a power level by chance fluctuation assuming the Gaussian white noise were calculated based on method provided by Lomb (1976) and Scargle (1982). And their values are 1.20×10^{-17} and 4.21×10^{-15} , respectively. In our timing analysis, the number of independent frequencies (i.e., the trial factor) was calculated by $N = (f_{\max} - f_{\min})/\delta f = 96943$, where δf is frequency resolution determined by the length of the *Fermi*-LAT observations. Then the False Alarm Probability (FAP) is calculated by the form of $\text{FAP} = 1 - (1 - p_{\text{isp}})^N \sim p_{\text{isp}} \times N$, after taking into account the trial number N . And their FAPs are derived to be 1.16×10^{-12} and 4.09×10^{-10} for P_H and P_L , which corresponding to $\sim 7.1\sigma$ and $\sim 6.3\sigma$ confidence levels. In right panel of Figure 2, we show 5σ and 7σ confidence levels with red dashed and blue dashed-dotted lines, respectively. Interestingly, the HESS data reported by Aharonian et al. (2006) also present two potential signals with periods of 3.42(5) and 4.56(10) day, which are similar to the two signals reported here. The errors associated with these periods were derived from the full-widths at half-maximum of the power peaks. For easy reference, we also include a schematic of the results for LS 5039 in the inset of right panel of Figure 2, adapted from Aharonian et al. (2006).

Considering the broad point spread function of the *Fermi*-LAT, periodic signals from neighboring sources may also appear in the power spectrum of the target. From the residual TS map (right panel of Figure 1), we can see that there are no new γ -ray sources beyond those listed in the 4FGL-DR4. Therefore, we constructed power spectra for the two γ -ray sources closest to the target, 4FGL J1827.4–1445 and 4FGL J1829.4–1500, using the same process, and present them in Figure 3 with black and orange histograms, respectively. We observe a prominent peak corresponding to the P_{orb} of LS 5039, along with a weaker peak corresponding to its first harmonic. However, no signals corresponding to P_H and P_L are detected.

To test whether these two signals are energy-dependent, we constructed light curves in three energy bands, 0.1–0.3, 0.3–1.0, and 1.0–500.0 GeV, using the same aperture photometry method. Their power spectra are shown in Figure 4 with black, red, and green histograms, respectively. We observe that the peak values of these two new signals, as well as the orbital period signal, decrease as the energy increases across the three energy ranges.

2.3. Phase-resolved Analysis

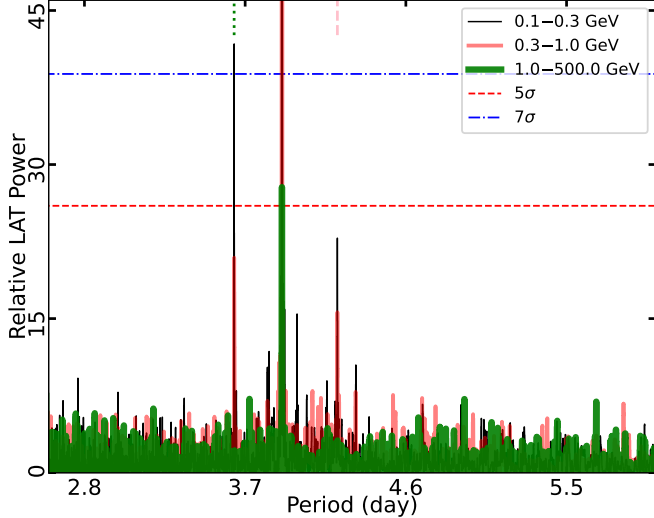


Figure 4. LS 5039’s energy-dependent LSP power spectra in 0.1–0.3, 0.3–1.0, and 1.0–500.0 GeV. The black, red, and green histograms stand for the spectra constructed with 0.1–0.3, 0.3–1.0, and 1.0–500.0 GeV AP light curves, respectively. As in Figure 2, the red dashed and blue dashed-dotted lines are 5σ and 7σ confidence levels.

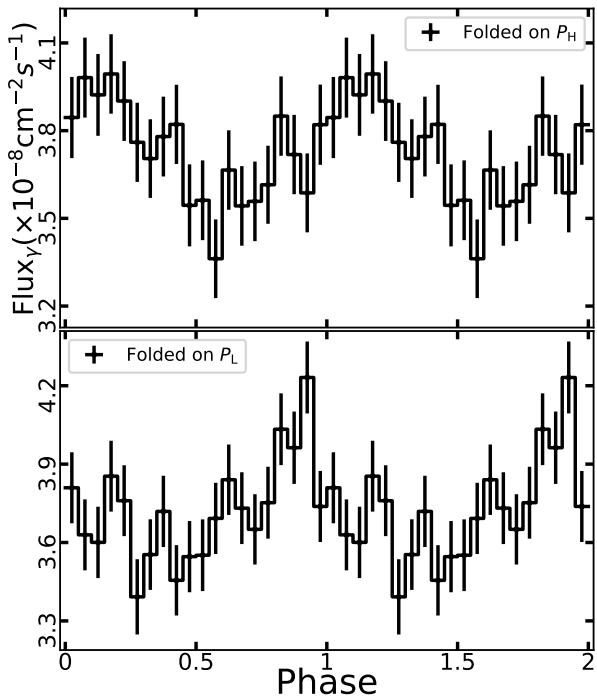


Figure 5. Phase-resolved light curves derived from the 0.1–500.0 GeV Fermi-LAT events, folded over the periods P_H (top panel) and P_L (bottom panel). Both panels share the same y-axis labels.

To examine the periodic profiles of the two signals, we derived phase-resolved light curves based on the periods of P_H and P_L by dividing the 0.1–500.0 GeV Fermi-LAT events into 20 phase intervals. For each phase interval, we performed a likelihood analysis to determine the fluxes, using phase zero at periastron and setting the reference epoch T_0 at MJD 51,942.59, as described by Casares et al. (2005b). We present the phase-resolved light curves for P_H and P_L in the upper and lower panels of Figure 5, respectively. These light curves clearly demonstrate periodic modulation profiles that differ from the modulation profile of the orbital period. Moreover, there are also significant differences between the profiles of P_H and P_L .

3. SUMMARY AND DISCUSSION

Here, we conducted a timing analysis using the LSP method on approximately 16 years of *Fermi*-LAT observations. Our analysis identified two new periodic signals with frequencies higher and lower than the orbital period (3.90609 day). These signals have periods of 3.63819 day and 4.21654 day, with confidence levels of 7.1σ and 6.3σ , respectively. Moreover, these new periodic signals share the same frequency interval as the orbital period. All three signals, including the two new periodic signals and the orbital period, show a trend of decreasing strength with increasing energy. This trend may be attributed to statistical factors, as there are much more γ -rays in lower energies than that in higher energies. Additionally, in previous studies, the HESS data appeared two potential signals with similar periods (Aharonian et al. 2006) to those we discovered in our Fermi-LAT analysis, which independently support the authenticity of our new findings. We know that in astrophysics, there are many causes that can produce periodic signals, but it is quite rare for two signals to have the same frequency interval. Considering that the P_H and P_L signals share the same interval as the orbital period in the frequency domain, we will discuss two scenarios that could generate these signals in the following discussion.

During timing analysis, peaks with the same frequency interval in the power spectrum can originate from the sidelobes of the main peak (i.e., the orbital period; Bloomfield 1976), caused by the finite length of observations and the use of windowing functions. These sidelobes are evenly distributed on both sides of the main peak, with their peak values gradually decreasing, which makes the first sidelobe the most likely candidates. In this scenario, we can obtain the locations of the first sidelobe using the formula: $P_{\text{sidelobe}} = P_{\text{orb}} \pm \frac{7}{5} P_{\text{orb}}^2 / T_{\text{obs}}$ in our timing analysis, where P_{sidelobe} is the periods corresponding to the first sidelobe, and T_{obs} is the length

of Fermi-LAT observations during the timing analysis. The values for the first sidelobes are calculated to be 3.902420 or 3.909765 day, which differ significantly from the P_H and P_L values. Therefore, we believe that the P_H and P_L signals cannot originate from the sidelobes of the orbital period of LS 5039. Additionally, if the two signals originated from the sidelobes, they should also appear in the power spectra of the two neighboring γ -ray sources. However, the power spectra of these two sources are significantly influenced by the orbital period of LS 5039, and they do not show the P_H and P_L signals. This further indicates that the P_H and P_L signals are related to LS 5039 and not associated with the sidelobes.

We then introduce an alternative scenario that could also produce two periodic signals with the same frequency interval. We propose that there may be a third body in the LS 5039 system, suggesting that LS 5039 could be a three-body system, as that reported in Ransom et al. (2014); Rebassa-Mansergas et al. (2022). The third body orbits the barycenter of the original binary system, with a hypothesized orbital period of P_{hyp} . And P_H and P_L signals likely originate from certain frequency combinations involving the P_{orb} and P_{hyp} . To simplify this process, we omit the phase shift parameters and assume that the P_{hyp} modulation has a sinusoidal function. And the γ -ray flux (F_γ) is modulated by a form of

$$F_\gamma = A \sin(2\pi t f_{\text{hyp}}) + C. \quad (1)$$

Since the P_{orb} signal is much stronger than the P_H and P_L in the power spectrum (Figure 2), hence we assume the amplitude (A) and constant (C) of P_{hyp} are strongly modulated by the main periodic signal (P_{orb}) and they have the forms of

$$A = A_1 \sin(2\pi t f_{\text{orb}}) + C_1 \quad (2)$$

and

$$C = A_2 \sin(2\pi t f_{\text{orb}}) + C_2. \quad (3)$$

Then we simplify this process again and assume $A_1 = A_2 = 1$ and $C_1 = C_2 = 0$. Then,

$$F_\gamma = 0.5 \{ \cos[2\pi t(f_{\text{orb}} - f_{\text{hyp}})] - \cos[2\pi t(f_{\text{orb}} + f_{\text{hyp}})] \} + \sin(2\pi t f_{\text{orb}}). \quad (4)$$

Consequently, we will see two peaks (with the corresponding frequencies to $f_H = f_{\text{orb}} + f_{\text{hyp}}$ and $f_L = f_{\text{orb}} - f_{\text{hyp}}$) around the orbital period in the power spectrum. The hypothesized period can be calculated as $P_{\text{hyp}} = \frac{1}{f_{\text{hyp}}} = \frac{2}{f_H - f_L} = 53.049(21)$ day, with the uncertainty derived from the propagation of errors in f_H and f_L .

Additionally, we note that *Fermi*-LAT operations can introduce artificial periodic signals (Atwood et al. 2009). One such signal, which is close to the P_{hyp} , corresponds to the *Fermi*-LAT's orbital precession period of 53.4 day¹, we indicate it in Figures 2 (left) and 3 by gray dashed-dotted lines. However, there are no peaks at this precession period in the power spectra of 4FGL J1826.2–1450 and the two neighboring γ -ray sources, and neither P_H or P_L appears in the power spectra of the neighboring sources. Therefore, we conclude that our light curves are not influenced by this precession period, furthermore the 53.4 day period does not fall within the uncertainties of P_{hyp} . Moreover, the HESS dataset also reveal two potential signals (Aharonian et al. 2006) with periods similar to those reported here. Thus, we infer that P_H or P_L are not related to the *Fermi*-LAT's orbital precession period.

Regardless, this discovery enhances our knowledge of LS 5039 and offers new insights into the dynamics and evolution of massive binary systems. The cause of these two new periodic signals remains uncertain. Further observations, particularly multi-wavelength ones, are encouraged to confirm the authenticity of the two periodic signals and to reveal their origins.

- 1 We would like to thank the anonymous referee for helpful
- 2 suggestions and Jian Li for useful comments. This work
- 3 is supported in part by the National Natural Science
- 4 Foundation of China under grant Grants Nos. 12233006,
- 5 U2031205, and 12163006, the Basic Research Program
- 6 of Yunnan Province No. 202201AT070137, and the
- 7 joint foundation of Department of Science and Tech-
- 8 nology of Yunnan Province and Yunnan University
- 9 No. 202201BF070001-020. P.Z. acknowledges the sup-
- 10 port by the Xingdian Talent Support Plan - Youth
- 11 Project.

¹ https://fermi.gsfc.nasa.gov/ssc/data/analysis/LAT_caveats_temporal.html

REFERENCES

- Abdo, A. A., Ackermann, M., Ajello, M., et al. 2009, *ApJL*, 706, L56, doi: [10.1088/0004-637X/706/1/L56](https://doi.org/10.1088/0004-637X/706/1/L56)
- . 2010, *ApJ*, 708, 1254, doi: [10.1088/0004-637X/708/2/1254](https://doi.org/10.1088/0004-637X/708/2/1254)
- Aharonian, F., Akhperjanian, A. G., Bazer-Bachi, A. R., et al. 2006, *A&A*, 460, 743, doi: [10.1051/0004-6361:20065940](https://doi.org/10.1051/0004-6361:20065940)
- Albert, J., Aliu, E., Anderhub, H., et al. 2006, *Science*, 312, 1771, doi: [10.1126/science.1128177](https://doi.org/10.1126/science.1128177)
- Atwood, W. B., Abdo, A. A., Ackermann, M., et al. 2009, *ApJ*, 697, 1071, doi: [10.1088/0004-637X/697/2/1071](https://doi.org/10.1088/0004-637X/697/2/1071)
- Ballet, J., Bruel, P., Burnett, T. H., Lott, B., & The Fermi-LAT collaboration. 2023, arXiv e-prints, arXiv:2307.12546, doi: [10.48550/arXiv.2307.12546](https://doi.org/10.48550/arXiv.2307.12546)
- Bloomfield, P. 1976, *Fourier analysis of time series: an introduction*
- Bykov, A. M., Petrov, A. E., Ponomaryov, G. A., Levenfish, K. P., & Falanga, M. 2024, arXiv e-prints, arXiv:2401.06271, doi: [10.48550/arXiv.2401.06271](https://doi.org/10.48550/arXiv.2401.06271)
- Cao, Z., Aharonian, F. A., An, Q., et al. 2021, *Nature*, 594, 33, doi: [10.1038/s41586-021-03498-z](https://doi.org/10.1038/s41586-021-03498-z)
- Casares, J., Ribas, I., Paredes, J. M., Martí, J., & Allende Prieto, C. 2005a, *MNRAS*, 360, 1105, doi: [10.1111/j.1365-2966.2005.09106.x](https://doi.org/10.1111/j.1365-2966.2005.09106.x)
- Casares, J., Ribó, M., Ribas, I., et al. 2005b, *MNRAS*, 364, 899, doi: [10.1111/j.1365-2966.2005.09617.x](https://doi.org/10.1111/j.1365-2966.2005.09617.x)
- Corbet, R. H. D., Chomiuk, L., Coe, M. J., et al. 2019, *ApJ*, 884, 93, doi: [10.3847/1538-4357/ab3e32](https://doi.org/10.3847/1538-4357/ab3e32)
- Fermi LAT Collaboration, Ackermann, M., Ajello, M., et al. 2012a, *Science*, 335, 189, doi: [10.1126/science.1213974](https://doi.org/10.1126/science.1213974)
- . 2012b, *Science*, 335, 189, doi: [10.1126/science.1213974](https://doi.org/10.1126/science.1213974)
- Hinton, J. A., Skilton, J. L., Funk, S., et al. 2009, *ApJL*, 690, L101, doi: [10.1088/0004-637X/690/2/L101](https://doi.org/10.1088/0004-637X/690/2/L101)
- Horne, J. H., & Baliunas, S. L. 1986, *ApJ*, 302, 757, doi: [10.1086/164037](https://doi.org/10.1086/164037)
- Johnston, S., Manchester, R. N., Lyne, A. G., et al. 1992, *ApJL*, 387, L37, doi: [10.1086/186300](https://doi.org/10.1086/186300)
- Kerr, M. 2011, *ApJ*, 732, 38, doi: [10.1088/0004-637X/732/1/38](https://doi.org/10.1088/0004-637X/732/1/38)
- Li, J., Torres, D. F., Cheng, K. S., et al. 2017, *ApJ*, 846, 169, doi: [10.3847/1538-4357/aa7ff7](https://doi.org/10.3847/1538-4357/aa7ff7)
- Lomb, N. R. 1976, *Ap&SS*, 39, 447, doi: [10.1007/BF00648343](https://doi.org/10.1007/BF00648343)
- Maíz Apellániz, J., Sota, A., Arias, J. I., et al. 2016, *ApJS*, 224, 4, doi: [10.3847/0067-0049/224/1/4](https://doi.org/10.3847/0067-0049/224/1/4)
- Moldón, J., Ribó, M., & Paredes, J. M. 2012, *A&A*, 548, A103, doi: [10.1051/0004-6361/201219553](https://doi.org/10.1051/0004-6361/201219553)
- Ransom, S. M., Stairs, I. H., Archibald, A. M., et al. 2014, *Nature*, 505, 520, doi: [10.1038/nature12917](https://doi.org/10.1038/nature12917)
- Rebassa-Mansergas, A., Xu, S., Raddi, R., et al. 2022, *ApJL*, 927, L31, doi: [10.3847/2041-8213/ac5a55](https://doi.org/10.3847/2041-8213/ac5a55)
- Scargle, J. D. 1982, *ApJ*, 263, 835, doi: [10.1086/160554](https://doi.org/10.1086/160554)
- Takahashi, T., Kishishita, T., Uchiyama, Y., et al. 2009, *ApJ*, 697, 592, doi: [10.1088/0004-637X/697/1/592](https://doi.org/10.1088/0004-637X/697/1/592)
- Weng, S.-S., Qian, L., Wang, B.-J., et al. 2022, *Nature Astronomy*, 6, 698, doi: [10.1038/s41550-022-01630-1](https://doi.org/10.1038/s41550-022-01630-1)
- Yoneda, H., Makishima, K., Enoto, T., et al. 2020, *PhRvL*, 125, 111103, doi: [10.1103/PhysRevLett.125.111103](https://doi.org/10.1103/PhysRevLett.125.111103)
- Zechmeister, M., & Kürster, M. 2009, *A&A*, 496, 577, doi: [10.1051/0004-6361:200811296](https://doi.org/10.1051/0004-6361:200811296)
- Zhang, P. 2024, *ApJ*, 972, 80, doi: [10.3847/1538-4357/ad6a16](https://doi.org/10.3847/1538-4357/ad6a16)